Endomembrane mutiny: how picornaviruses hijack host organelles to support their replication

Melia, C.E.

CHAPTER 3

ESCAPING HOST FACTOR PI4KB INHIBITION: ENTEROVIRUS GENOMIC RNA REPLICATION IN THE ABSENCE OF REPLICATION ORGANELLES

Charlotte E. Melia[1$], Hilde M. van der Schaar[2$], Heyrhyoung Lyoo[2], Ronald W.A.L. Limpens[1], Qian Feng[2†], Maryam Wahedi[2], Gijs J. Overheul[3], Ronald P. van Rij[3], Eric J. Snijder[4], Abraham J. Koster[1], Montserrat Bárcena[1&], Frank J.M. van Kuppeveld[2&]

Published in Cell Reports 2017. 21;3: 587-599
DOI: 10.1016/j.celrep.2017.09.068

[1] Department of Molecular Cell Biology, Leiden University Medical Center, Leiden, 2333 ZC, The Netherlands

[2] Department of Infectious Diseases & Immunology, Utrecht University, Utrecht, 3584 CL, The Netherlands

[3] Department of Medical Microbiology, Radboud Institute for Molecular Life Sciences, Nijmegen, 6525 GA, The Netherlands

[4] Department of Medical Microbiology, Leiden University Medical Center, Leiden, 2333 ZA, The Netherlands

[†]Current address: Institute of Biochemistry, ETH Zürich, 8093 Zürich, Switzerland

[$,&]These authors contributed equally

SUMMARY

Enteroviruses reorganize cellular endomembranes into replication organelles (ROs) for genome replication. Although enterovirus replication depends on phosphatidylinositol 4-kinase type III beta (PI4KB), its role, and that of its product PI4P, is only partially understood. Exploiting a mutant coxsackievirus resistant to PI4KB inhibition, we uncover that PI4KB activity has distinct functions in proteolytic processing of the viral polyprotein and in RO biogenesis. The escape mutation rectified a proteolytic processing defect imposed by PI4KB inhibition, pointing to a possible escape mechanism. Remarkably, under PI4KB inhibition the mutant virus could replicate its genome in the absence of ROs, using instead the Golgi apparatus. This impaired RO biogenesis provided an opportunity to investigate the proposed role of ROs in shielding enteroviral RNA from cellular sensors. Neither accelerated sensing of viral RNA nor enhanced innate immune responses were observed. Together, our findings challenge the notion that ROs are indispensable for enterovirus genome replication and immune evasion.

INTRODUCTION

Positive-strand RNA (+RNA) viruses comprise many human pathogens, such as hepatitis C virus, Zika virus, dengue virus, SARS- and MERS-coronavirus, and enteroviruses. Despite substantial genetic divergence across virus families, some features of replication are common to all +RNA viruses infecting eukaryotes. One of the most striking is the remodelling of host cell endomembranes into novel membranous compartments in the cytoplasm of the infected cell. These compartments serve as compositionally unique platforms upon which the components of the viral RNA synthesis machinery assemble, and whose micro-environments may facilitate efficient genome replication (reviewed in (1) and (2)). In addition, they have been postulated to play a role in the evasion of the innate antiviral host responses by shielding viral RNA products from cytosolic sensors such as MDA5 and RIG-I, which signal to activate the type I interferon (IFN-a/b) pathway, and protein kinase R (PKR), which activates an integral stress response (3, 4).

Members of the Enterovirus genus, belonging to the Picornaviridae family, include poliovirus, coxsackie A and B viruses, several numbered enteroviruses (e.g. EV-D68, EV-A71), and rhinoviruses, which are causative agents of various human diseases. Enteroviruses, like other positive-sense RNA viruses, modify host-cell membranes to form structures with novel morphologies. These modified membranes serve as platforms for viral replication, which we will refer to as replication organelles (ROs). At earlier stages of coxsackievirus B3 (CVB3) or poliovirus (PV) infection, ROs emerge as single-membrane tubules that appear to form at the expense of the Golgi apparatus. These tubules are interspersed with double-membrane vesicles (DMVs), which are believed to arise as tubules deform and enwrap small volumes of cytosol. In this way, most tubules transform into DMVs over the course of infection, and DMVs may be further enwrapped to form multilamellar vesicles (5, 6). Each stage of virus replication, including the transformation of cellular membranes into ROs, is dependent upon the interplay between viral proteins and host factors. The small, membrane-anchored enterovirus 3A protein has a key role in generating ROs (7), and is known to recruit host factors that are essential for genome replication. One of these factors is phosphatidylinositol 4-kinase type IIIβ (PI4KB) (8, 9). In uninfected cells PI4KB is a Golgi-resident enzyme that generates

phosphatidylinositol 4-phosphate (PI4P), while during enterovirus infection the viral 3A protein recruits PI4KB to ROs, enriching them in PI4P (8, 10).

The importance of PI4P in viral infections has been the subject of several recent investigations, both for the Picornaviridae, such as Aichivirus (genus Kobuviruses) and encephalomyocarditis virus (EMCV) (genus Cardiovirus) and for other +RNA viruses, such as hepatitis C virus (HCV) (reviewed in (11) and (12)). In uninfected cells, PI4P is involved in a multitude of functions, including signalling, membrane trafficking, regulation of Golgi apparatus organisation, and lipid homeostasis (reviewed in (13) and (14)). Of particular relevance for viruses that utilise PI4P is the counterflux of PI4P and cholesterol between Golgi apparatus and ER, which is mediated by the oxysterol-binding protein (OSBP). OSBP acts as a bridge between these two membrane compartments to generate a membrane contact site, using PI4P as a Golgi-based anchor and vesicle-associated membrane protein-associated protein A (VAP-A) as an ER anchor (15). During enterovirus infection, OSBP is diverted to create a novel type of membrane contact site between ROs and the ER. These sites mediate the exchange of PI4P for cholesterol, which is another essential lipid for enterovirus genome replication (16-18).

Recruitment of PI4KB by the viral 3A protein is critical for enterovirus genome replication (8, 9), but its exact role is unclear. The stage of genome replication in the enterovirus life cycle encompasses different processes, including proteolytic processing of the polyprotein, RO biogenesis, and RNA synthesis by the viral replication machinery. In this study, we used a CVB3 mutant resistant to PI4KB inhibition, i.e. CVB3 3A-H57Y (19), to further dissect the role of PI4KB and the PI4P-rich environment it generates during genome replication. We show that PI4KB activity facilitates efficient proteolytic processing of the CVB3 polyprotein. The 3A-H57Y substitution compensates for the impairment of polyprotein processing caused by PI4KB inhibition, which may represent the escape mechanism of this mutant virus. Distinct from its effect on polyprotein processing, we found that PI4KB inhibition also delayed RO formation. Remarkably, CVB3 3A-H57Y could replicate its genome in the absence of detectable ROs when PI4KB was inhibited. Under these conditions, viral RNA synthesis was observed instead at a cellular organelle, the Golgi apparatus, which challenges the notion that ROs are essential for the exponential phase of genome replication. Golgi disintegration and RO formation did eventually occur under PI4KB inhibition, which suggests that PI4KB activity is not fundamentally required for RO biogenesis, but expedites the process. The delay in RO formation under PI4KB inhibition was exploited to experimentally test the hypothesis that ROs shield viral RNA from cytoplasmic sensors of the innate immune system. Our results suggest that, in addition to being dispensable for viral RNA synthesis, enterovirus ROs do not play a pivotal role in suppression of the innate antiviral response pathways.

RESULTS

CVB3 3A-H57Y RO formation is impaired under PI4KB inhibition

First, we set out to study the morphology of the ROs induced by CVB3 3A-H57Y under conditions where PI4KB is not inhibited. Infected BGM cells were prepared for electron microscopy (EM) by high-pressure freezing and freeze-substitution at different times post-infection and analysed for the presence of membrane modifications. The first ROs induced by CVB3 3A-H57Y were detected at 5 hours post infection (hpi). At this stage single-membrane tubules were predominant,

interspersed with double-membrane vesicles (DMVs) (Fig. 1A). The emergence of ROs coincides with disintegration of the Golgi apparatus in wt infection (5) and, concordantly, the Golgi apparatus was not observed in cell sections that contained ROs at any time point in this analysis. Later in infection tubules had largely transformed into DMVs (Fig. 1A, 6 hpi) and into multilamellar structures (Fig. 1A, 7 hpi). This progression closely reflects observations of wt CVB3 RO development with regard to both the specific morphologies induced and the time frame over which they develop (5), (Fig. S1A). Together, these results indicate that the 3A-H57Y substitution does not affect RO development or their general architecture.

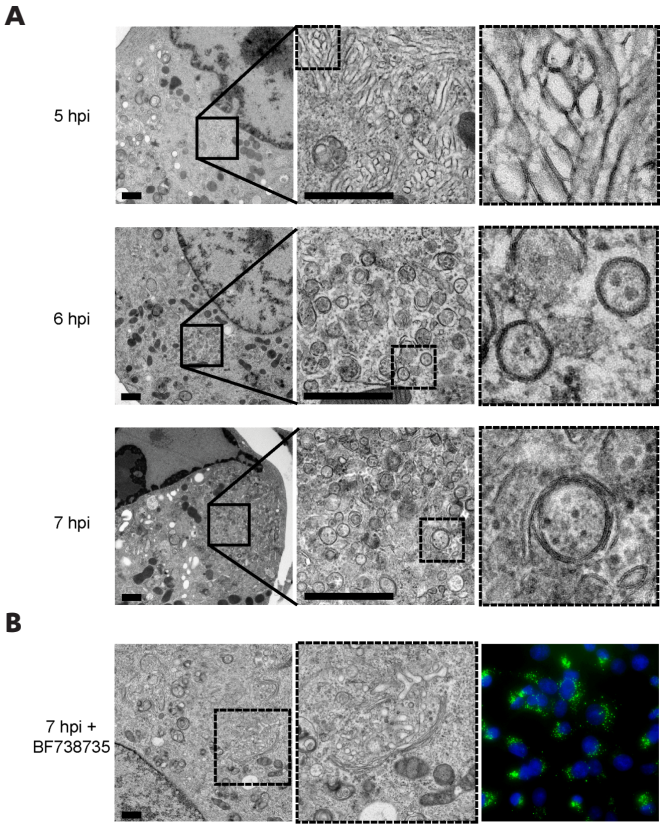

Figure 1. CVB3 3A-H57Y RO formation is impaired under PI4KB inhibition. A, B) BGM cells infected with CVB3 3A-H57Y (MOI 50). A) Cells fixed for EM analysis at early (5 hpi), intermediate (6 hpi) or late (7 hpi) stages of infection show the progression in RO development. B) ROs were not observed in EM cell sections (up to 8 hpi, n = 153) from cells treated with BF738735. (Left) An example of the Golgi apparatus in cells fixed at 7 hpi. (Right) Parallel immunofluorescence data (dsRNA (green) and nuclear stain (blue). Scale bars, 1 µm. See also Figs. S1 and S2.

Next, we investigated the effect of PI4KB inhibition on RO development during CVB3 3A-H57Y infection. To determine suitable time points for EM analysis of cells infected in the presence of a PI4KB inhibitor, we first measured viral replication in the presence of BF738735, a potent and specific PI4KB inhibitor without overt cytotoxicity (a.k.a. Compound 1; (9, 20)). Unlike CVB3 wt (Fig. S2A), CVB3 3A-H57Y was resistant to BF738735 (Fig. S2B), although its replication was nevertheless delayed and impaired in the presence of BF738735 with regard to both viral RNA (vRNA) and infectious

progeny virus. This is in agreement with observations using other PI4KB inhibitors (e.g. PIK93; (19)). To examine whether the impairment of replication upon PI4KB inhibition was the consequence of a decrease in the number of infected cells and/or a reduced level of vRNA replication, we collected cells infected with EGFP-CVB3 3A-H57Y at different time points post infection and analysed them with flow cytometry. PI4KB inhibition reduced the number of CVB3 3A-H57Y-infected cells (by ~3-fold), delayed replication (by ~1-2 h), and limited viral protein production, as reflected by reduced EGFP levels (Fig. S2C). These results indicate that the PI4KB inhibitor imposes a critical barrier to CVB3 3A-H57Y replication in a subpopulation of cells, and reduces the efficiency of replication in those cells where infection is established.

Based on the growth curve analysis, cells were fixed and processed for EM between 5 and 8 hpi, as this period encompasses the exponential phase of vRNA replication for CVB3 3A-H57Y under PI4KB inhibition. Remarkably, while ROs were detected at a frequency of ~50% in EM cell-sections from infections in the absence of PI4KB inhibitor (n = 43 cell-sections assessed at 6 hpi), neither archetypal enterovirus ROs (i.e. clusters of single-membrane tubules and/or DMVs) nor cellular membranes with atypical morphologies were detected in cells infected under PI4KB inhibition (n = 153 cell-sections), even at late time points (7-8 hpi, n = 47 cell-sections, example shown in Fig. 1B). Seemingly intact Golgi cisternae were apparent in these cells and were detected at a frequency similar to that of mock-infected or BF738735-treated cells (Fig. S1B and C respectively). Corresponding immunofluorescence microscopy data showed a high percentage of cells positive for dsRNA labelling, confirming that the lack of membrane modifications in the EM analysis was not simply due to a low number of infected cells (Fig. 1B, right). These data show that RO development is impaired by PI4KB inhibition, and suggest that replication may be taking place instead at a cellular organelle.

CVB3 3A-H57Y replicates its genome at the Golgi apparatus under PI4KB inhibition

As an initial indicator of the replication site under PI4KB inhibition, we performed immunofluorescence microscopy on infected cells (Fig. 2A). Cells were fixed at 5 hpi in the absence of inhibitor, and at 6 hpi in the presence of inhibitor given the delay in replication. Similar to findings for wt virus (8, 19), both 3A and dsRNA were detected throughout the cytoplasm in cells infected with CVB3 3A-H57Y in the absence of PI4KB inhibition (Fig. 2A, left panels). Golgi disassembly could be readily visualized through the signal reduction and dispersion of the cis-Golgi marker GM130 and the trans-Golgi network marker TGN46, whereas the PI4KB signal overlapped with the 3A labelling. Upon PI4KB inhibitor treatment however, 3A and dsRNA were primarily confined to the perinuclear region (Fig. 2A, right panels). In wide-field images, the strength and distribution of GM130 and TGN46 signals were largely maintained and overlapped with the viral 3A signal. These results suggested that both the 3A-H57Y protein and dsRNA reside at the Golgi apparatus in the presence of inhibitor. To confirm that these observations were due to specific inhibition of PI4KB, the localisation of 3A-GFP was assessed using different PI4KB inhibitors. Similar to BF738735, enviroxime, GW5074 or PIK93 treatment resulted the accumulation of 3A specifically at the Golgi region, although confocal imaging revealed that 3A did not directly co-localise with the cis-Golgi marker GM130 (Fig. 2B).

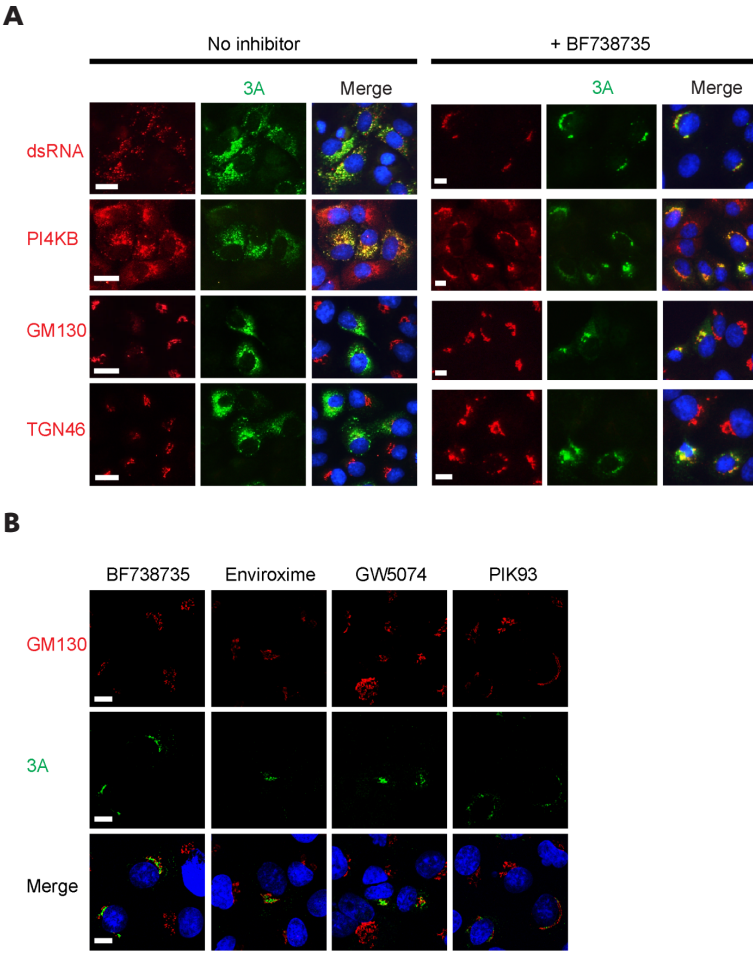

Figure 2. The 3A protein localises to the Golgi apparatus under PI4KB inhibition. A, B) BGM cells infected with CVB3 3A-H57Y (MOI 10). Untreated cells were fixed at 5 hpi ((A) left panels) and drug treated cells were fixed at 6 hpi ((A) right panels, and (B)). Fixed cells were labelled with the indicated antibodies and a nuclear stain (blue). Scale bars, 10 µm.

To unambiguously determine the subcellular location of the 3A-H57Y protein under PI4KB inhibitor treatment, correlative light and electron microscopy (CLEM) was performed. For this we employed the split-GFP system (21) to label the 3A-H57Y protein, in a similar approach to that previously reported for wt CVB3 (22). To produce a split-GFP CVB3 3A-H57Y mutant, the final beta sheet of GFP, i.e. strand 11, further referred to as GFP(S11), was introduced into the 3A-H57Y protein to produce CVB3 3A-H57Y(S11). Upon CVB3 3A-H57Y(S11) infection of BGM cells stably expressing the remaining portion of GFP (GFPS1-10), the two fragments of GFP self-assemble to produce GFP-tagged 3A-H57Y. GFP-tagged 3A-H57Y was then visualized by confocal microscopy before chemical fixation and processing for EM. Overlays of 3A-H57Y-GFP signal with the corresponding EM cell-sections fixed at 6 hpi revealed that the 3A protein localised specifically to the Golgi apparatus (Fig. 3A).
The presence of the 3A-H57Y protein at the Golgi apparatus suggested that vRNA replication occurs

at this compartment under PI4KB inhibition. To further investigate this, metabolic labelling was performed to detect newly synthesized vRNA in situ. Infected cells were pre-treated with 10 µg/ml dactinomycin to inhibit cellular transcription, and incubated with tritiated uridine for 45 minutes prior to fixation to label newly-synthesised vRNA. As a control, mock-infected cells underwent the same treatment. After processing for EM, radiolabelled uridine was detected by autoradiography (ARG). In cells infected with CVB3 3A-H57Y without PI4KB inhibition, abundant ARG signal was found in regions containing typical ROs (Fig. 3B). Although RO membranes in chemically fixed samples appeared somewhat distended in comparison to high-pressure frozen material (see Fig. 1), they were recognisable as clusters of single-membrane compartments (Fig. 3B, black arrowhead)

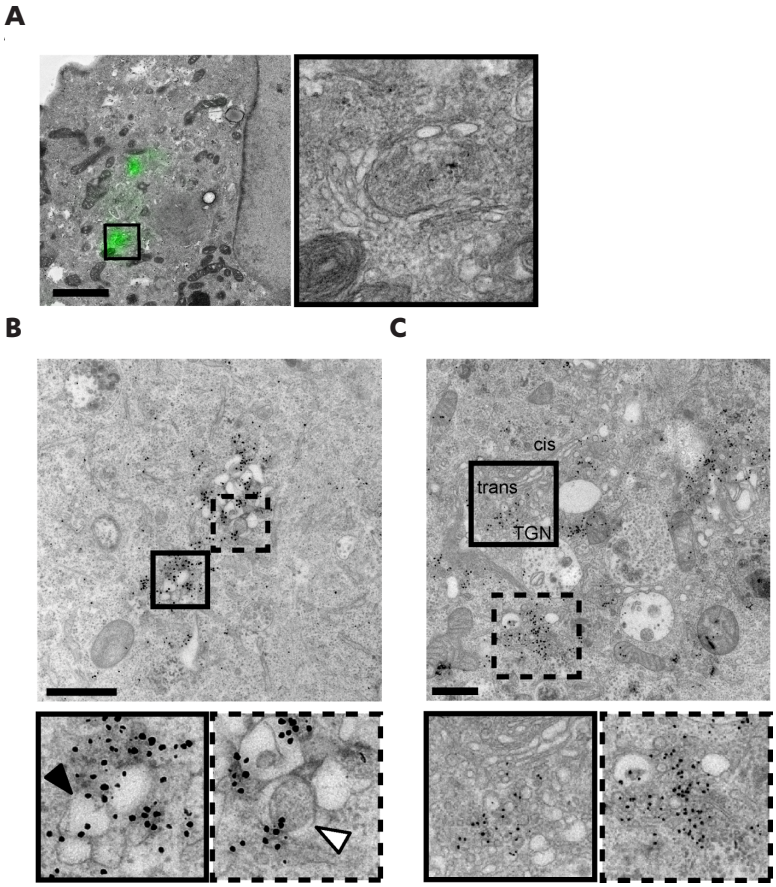

Figure 3. Replication under PI4KB inhibition occurs at the Golgi apparatus. A) BGM(GFPS1-10) cells infected with CVB3 3A-H57Y(S11) (MOI 7) monitored by live-cell LM, fixed at 6 hpi, and processed for CLEM. Overlay of the 3A-GFP signal at the time of fixation with the corresponding EM image (left). Inset highlights one of two 3A-GFP foci present in the image shown, both of which correspond to Golgi membranes. B, C) BGM cells infected with CVB3 3A-H57Y (MOI 50), metabolically labelled, fixed at 6 hpi (B) or 7 hpi (C), and processed for EM autoradiography to detect newly-synthesized vRNA (ARG). ARG signal is apparent as electron-dense grains. B) ROs positive for ARG signal were readily observed in the absence of BF738735. C) In cells treated with BF738735 ROs were not observed, and clusters of ARG signal were found exclusively at the Golgi apparatus. cis = Golgi apparatus cis face, trans = Golgi apparatus trans face, TGN = trans Golgi network. Scale bars, 2 µm (A) or 1 µm (B, C).

interspersed with DMVs (Fig. 3B, white arrowhead) that closely resemble the ROs observed in chemically fixed PV-infected (6, 23) or wt CVB3-infected cells (22). In CVB3 3A-H57Y-infected cells treated with PI4KB inhibitor and fixed at 7 hpi ROs were not observed (n = 148 cell sections), and abundant ARG signal was found at the Golgi apparatus (Fig. 3C), with the vast majority of signal localising to the trans-side of the Golgi apparatus and trans-Golgi network rather than the Golgi cisternae. This demonstrates that, under PI4KB inhibition, CVB3 3A-H57Y can replicate its genome

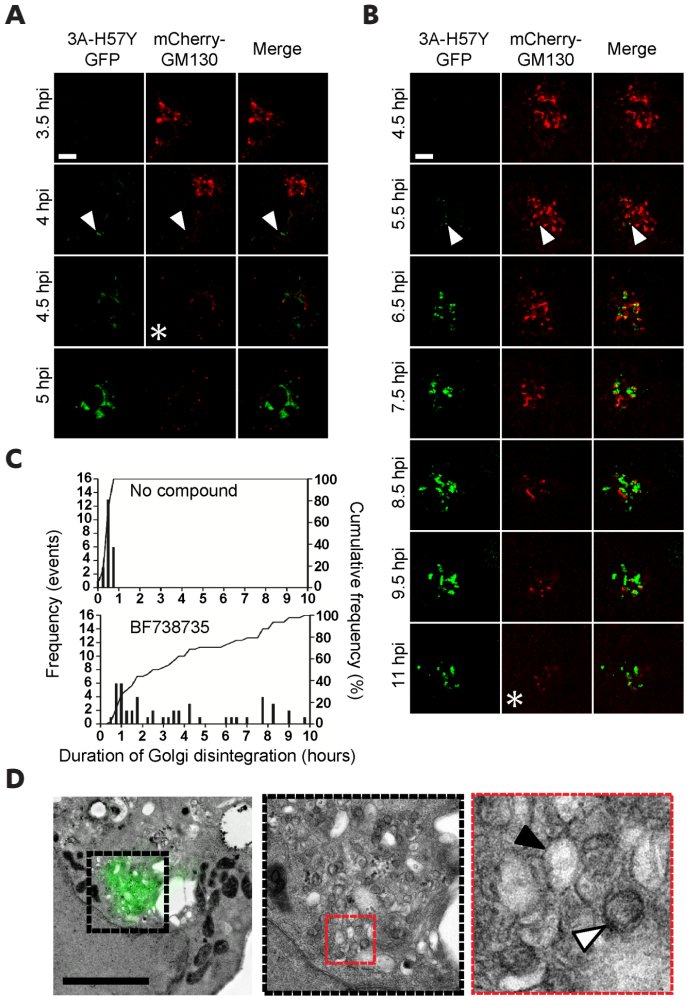

Fig. 4. Golgi disintegration during CVB3 3A-H57Y infection is prolonged under PI4KB inhibition, and ultimately results in RO formation. BGM(GFPS1-10) cells transduced with MLV mCherry-GM130, infected with CVB3 3A-H57Y(S11) (MOI 7) and imaged by live-cell confocal microscopy in the absence (A) or presence (B, D) of BF738735. Asterisks (A, B) denote completion of Golgi disintegration, evidenced by an entirely punctate mCherry-GM130 signal. A) Initial 3A-GFP signal was detected primarily at peripheral locations (arrowhead) and Golgi disintegration was typically complete within 25 minutes of its onset (C, upper graph n = 23 cells). B) In cells treated with BF738735, initial 3A-GFP signal was detected primarily at the Golgi apparatus (arrowhead). The Golgi disintegration duration was typically prolonged but highly variable (C, lower graph n = 48 cells). D) Cells were fixed for EM analysis at 9 hpi. The LM-EM overlay reveals single-membrane (black arrowhead) and double-membrane (white arrowhead) structures positive for 3A-GFP signal. Scale bars, 5 µm (D). See also Fig. S3.

in the absence of ROs on a seemingly intact Golgi apparatus.

Under PI4KB inhibition, ROs form late in CVB3 3A-H57Y-infected cells

Our results thus far show that, under PI4KB inhibition, CVB3 3A-H57Y replication is possible in association with an apparently intact cellular organelle. We next set out to establish whether PI4KB inhibition precludes Golgi disintegration and RO development entirely, or simply delays the process. Confocal microscopy of live cells expressing mCherry-GM130 was performed to monitor the Golgi apparatus across the course of CVB3 3A-H57Y(S11) infection, either with or without BF738735 treatment (Fig. 4A-C). In the absence of inhibitor, the process of Golgi fragmentation following CVB3 3A-H57Y(S11) infection was similar to that of wt split-GFP CVB3 infections (22). The onset of Golgi fragmentation occurred in conjunction with or even preceded 3A protein accumulation in the Golgi area, and Golgi disintegration was typically complete within 25 min (n = 23 cells) (Fig. 4A and C, upper graph). While in the absence of PI4KB inhibition early 3A signal was often located at peripheral foci (Fig. 4A arrowheads), under PI4KB inhibition the first 3A signal was often found in the Golgi region (Fig. 4B, arrowheads). Remarkably, the Golgi apparatus of most CVB3 3A-H57Y(S11) infected cells did disassemble during infections under PI4KB inhibition, but with markedly different dynamics. The onset of disintegration under these conditions did not coincide with 3A protein accumulation at the Golgi, but suffered a relative average delay of 30 minutes (n = 48 cells). Additionally, the time needed for Golgi disintegration was highly variable under PI4KB inhibition. In a minority of infected cells treated with BF738735 Golgi disassembly was as rapid as in untreated cells. However, in most cells the Golgi disintegration process was substantially prolonged (by up to 10 hours) under PI4KB inhibition (Fig. 4B and C, lower graph).

To determine whether Golgi disassembly under PI4KB inhibition was associated with the development of ROs, CLEM was performed on cells infected with split-GFP 3A-H57Y(S11) virus under BF738735 treatment and fixed at 9 hpi. While some cells retained seemingly intact Golgi membranes at this late stage in infection, in those cells lacking recognisable Golgi membranes the 3A-GFP signal was found at structures resembling typical early ROs (Fig. 4D, see Fig. 3A for comparison). As verified by immunofluorescence microscopy, PI4P did not accumulate in cells infected under PI4KB inhibition (Fig. S3), suggesting that the ROs that develop during CVB3 3A-H57Y infection under PI4KB inhibition do so independently of high PI4P levels.

PI4KB activity drives rapid Golgi disassembly and RO formation

RO formation is likely associated with the amount of viral protein produced in the cell, which in turn depends upon vRNA replication levels. Therefore, rather than the absence of high PI4P levels, the delay in CVB3 3A-H57Y vRNA replication under PI4KB inhibition could be solely responsible for impeding RO formation. Previously it was shown that replication-independent expression of PV non-structural proteins results in membranous structures reminiscent of ROs produced upon infection (24). Here, we engineered a replication-independent CVB3 expression system, which produces high amounts of viral proteins in the absence of vRNA replication. Hence, the inhibition of vRNA replication caused by PI4KB inhibition will not result in a delay in viral protein production in this setup. The system utilizes a CVB3 cDNA placed under the control of the bacteriophage T7 RNA polymerase, and is rendered replication-incompetent through modifications to the cloverleaf structure in the 5' untranslated region (UTR) of the viral genome that prevent replication via the

CVB3 polymerase (25). The 3A-H57Y substitution was introduced into this replication-incompetent CVB3 cDNA. Transfection of the CVB3 3A-H57Y cDNA plasmid in HuH-7/T7 cells, which stably express the T7 RNA polymerase, resulted in the expression of individual viral proteins whose amounts were not affected by the addition of PI4KB inhibitor (Fig. S4). Immunofluorescence analysis of transfected cells showed that the first 3A signal could be detected as early as 3 h post transfection (hpt), but without significant effects on the Golgi apparatus. In the absence of PI4KB inhibitor, Golgi disintegration was observed from 4 hpt onwards, as evidenced by the change in GM130 signal in transfected cells (Fig. 5A, upper panels). Under PI4KB inhibition Golgi disintegration was delayed by ~1 h (Fig. 5A middle and lower panels). While Golgi disintegration in the replication-independent system is more rapid than during infection (see Fig. 4), most likely because of the high protein expression levels generated with this system, these data nevertheless demonstrate that in cells with equal levels of viral proteins, PI4KB inhibition delays enterovirus-induced Golgi apparatus disassembly. To determine the contribution of the 3A-H57Y substitution to (delayed) Golgi disassembly, we examined whether the wt CVB3 cDNA could also induce Golgi disassembly under PI4KB inhibition in the replication-independent system. The results closely resembled those obtained for CVB3 3A-H57Y cDNA both with and without PI4KB inhibition (Fig. 5B). This demonstrates that the 3A-H57Y substitution does not affect Golgi disintegration.

Altogether, these findings strongly suggest that enterovirus RO biogenesis is driven by PI4KB activity.

The 3A-H57Y substitution rectifies a proteolytic polyprotein processing impairment induced by PI4KB inhibition

Another important step in the enterovirus replication cycle that relies on membranes is the proteolytic processing of the polyprotein by the viral proteases (26). Proteolytic polyprotein processing is a co- and post-translational event mediated by the viral proteinases 2Apro, 3Cpro, and 3CDpro. These proteinases catalyse a cascade of cleavages in cis and in trans that liberate individual capsid proteins, as well as replication proteins and their precursors (e.g. 2BC, 3AB and 3CD). Recent studies indicate that alterations to the lipid composition of membranes during PV infection impact polyprotein processing efficiency (27-29). Given that wt virus replication is abolished under PI4KB inhibition, we used the replication-independent CVB3 expression system to study the effects of PI4KB inhibition on polyprotein processing. Cells were lysed at 16 hours post transfection (hpt) and processed for Western blot analysis. PI4KB inhibition led to a relative accumulation of 3AB and a reduction in 3A for the wt polyprotein (Fig 5C, left). Remarkably, the 3A-H57Y substitution rectified this impaired polyprotein processing, as the relative levels of 3AB and 3A were not affected by PI4KB inhibition (Fig. 5C, right). PI4KB inhibition did not affect levels of 3CD or 3D. Together, these results demonstrate that PI4KB activity is important for proteolytic processing at the 3A-3B junction, but not at the 3C-3D junction (nor at the 2C-3A and 3B-3C junctions). The 3A-H57Y substitution restores processing to the level detected in the absence of inhibitor, which may point to a potential strategy of the mutant virus to escape PI4KB inhibition.

The delay in RO formation under PI4KB inhibition does not elicit a strong antiviral response

One of the proposed advantages of ROs is that they may shield vRNA products against viral RNA sensors present in the cytoplasm, such as MDA5, RIG-I, and PKR. Given that CVB3 3A-H57Y is

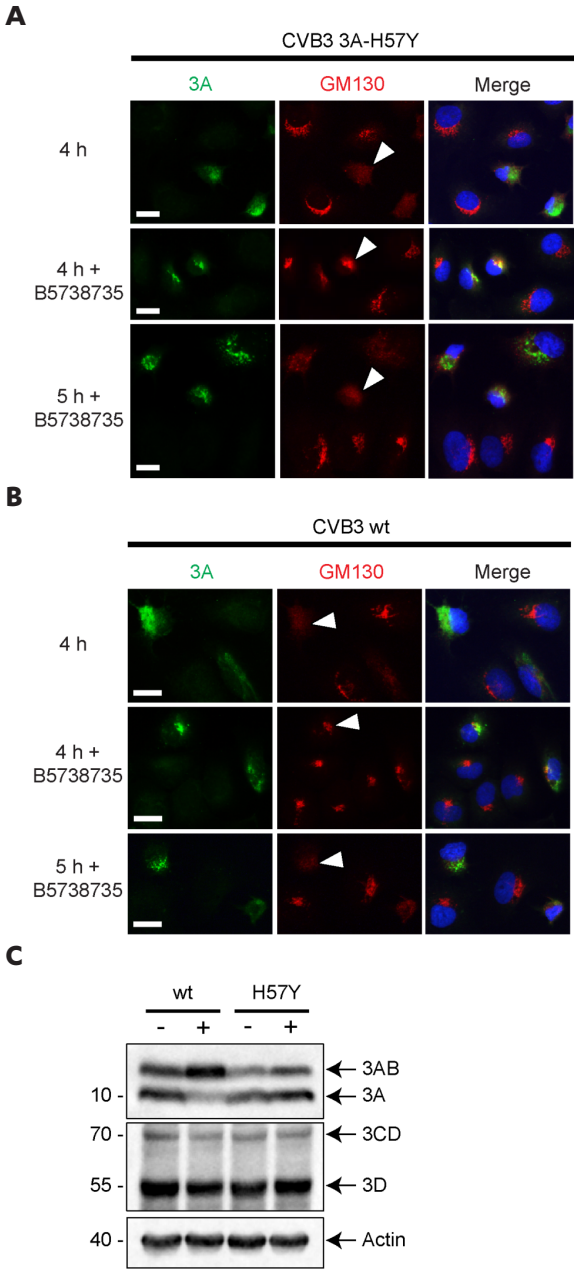

Figure 5. Effect of PI4KB inhibition on enterovirus-induced Golgi disintegration and proteolytic polyprotein processing in a replication-independent CVB3 system. HuH-7/T7 cells transfected with CVB3 3A-H57Y or wt CVB3 cDNA under the control of a T7 promoter, both rendered replication-incompetent by altering the 5'UTR of the genome. Where indicated, cells were treated with BF738735. A, B) Cells fixed at 4 h or 5 h post-transfection and labelled for 3A (green) and GM130 (red) alongside a nuclear stain (blue). Representative 3A-positive cells are indicated (arrowheads). Scale bars, 20 µm. C) Western blot analysis of lysates from cells at 16 h post-transfection using antibodies against 3A or 3D. Actin was used as a loading control. See also Fig. S4

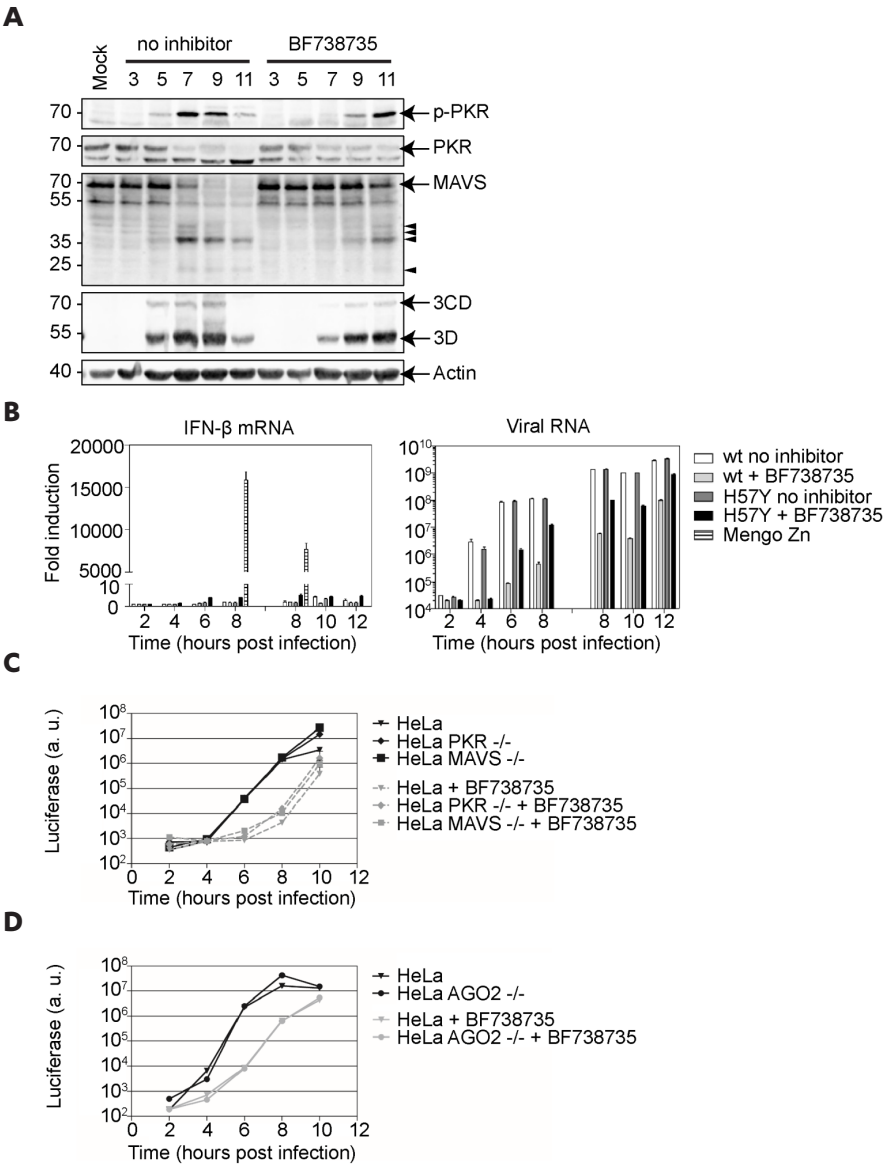

Fig. 6. Innate antiviral responses during CVB3 3A-H57Y infection. Cells infected and treated with BF738735 where indicated. A) HeLa cells infected with CVB3 3A-H57Y (MOI 50) were lysed for Western blot analysis at the indicated time points. Band sizes (in kDa), full-length proteins (arrows), and putative cleavage products (arrowheads) are indicated. B) HeLa cells infected with CVB3 wt or CVB3 3A-H57Y (MOI 10). Total RNA was isolated from cells and subjected to reverse transcription-quantitative PCR for interferon-b (IFN-b). Mengo Zn, whose L protein contains substitutions that render it unable to suppress IFN-b induction, was included as a positive control (left graph). Viral RNA levels were determined by quantitative RT-PCR (right graph). Data were normalized to actin mRNA levels. Results are expressed as fold induction relative to quantities in mock-infected cells. Two independent experiments are shown, ranging from 2-8 hpi and 8-12 hpi. C, D) Cells were infected with CVB3-Rluc 3A-H57Y (MOI 0.01) and lysed to determine the intracellular luciferase levels. Values represent mean values of triplicates ± standard error of the means. See also Figs. S5 and S6.

able to replicate its genome at the Golgi apparatus under PI4KB inhibition, vRNA products may be more accessible and better detected in this situation, thereby triggering an antiviral response that might limit or delay replication. To investigate whether viral dsRNA is better sensed under PI4KB inhibition, we studied the activation status of the cytoplasmic RNA sensor PKR. Western blot analyses were performed on infected cell lysates to assess viral protein levels in parallel with dsRNA-activated, phosphorylated PKR (p-PKR). The first appearance and the final levels of viral proteins were delayed and reduced respectively under PI4KB inhibition, which is in agreement with the observed reduction in the proportion of infected cells and the decrease in viral protein per cell (see Fig. S2C). Nevertheless, p-PKR emerged concomitantly with the accumulation of viral proteins both in the presence and absence of PI4KB inhibitor (Fig. 6A), suggesting that delayed RO formation under PI4KB inhibition does not lead to premature activation of PKR.

Another innate antiviral response that is activated upon sensing of vRNA products is the type I interferon (IFN-a/b) pathway. Enteroviruses counteract the transcription of IFN-a/b genes by cleaving components in the signalling pathways that control their activation, such as MDA5 (30) and its downstream adaptor MAVS (30, 31). The altered location of genome replication under PI4KB inhibition may influence the ability of the viral proteinases to cleave these components. However, we found that the appearance of MAVS degradation products in infected cell lysates coincided with the accumulation of viral proteins irrespective of the presence of PI4KB inhibitor (Fig. 6A). Furthermore, qPCR analysis showed that no substantial IFN-b response was triggered in infected cells in both conditions (Fig. 6B). Together, these results indicate that the delayed formation of ROs during infection does not accelerate cellular sensing of viral dsRNA, nor does it affect the ability of the viral proteinases to cleave MAVS.

As a complementary approach to investigate whether the delay in replication in the presence of PI4KB inhibitor is related to activation of innate antiviral responses, the level of CVB3 3A-H57Y replication was determined in cells lacking sensors of these pathways. Knock-out cells for PKR or MAVS, generated with CRISPR-Cas9 technology, were infected with CVB3 wt or 3A-H57Y that also encode Renilla luciferase as a sensitive measure to quantify the level of viral replication. In the absence of inhibitor, CVB3 3A-H57Y replicated to a similar extent in HeLa, HeLa PKR -/-, or HeLa MAVS-/- cells (Fig. 6C and S6). In the presence of PI4KB inhibitor, CVB3 3A-H57Y replication was delayed not only in HeLa cells, but also in PKR-/- or MAVS-/- cells. Thus, replication under PI4KB inhibition was not significantly increased in PKR-/- or MAVS-/- cells compared to parental HeLa cells. Similar results were obtained in U2OS cells, another human cell line (Fig. S5A and S6).

An alternative strategy employed by some eukaryotes, such as plants, worms, and insects, in response to viral infections is RNA interference (RNAi), although whether RNAi is an antiviral mechanism in mammalian cells remains controversial (32). In the RNAi pathway, the cytoplasmic sensor Dicer cleaves viral dsRNA into viral siRNAs, which are loaded by Argonaute-2 (AGO2) into the RNA-induced silencing complex (RISC) in order to degrade vRNA (33). Recently, it was reported that replication of the picornavirus EMCV was enhanced in mammalian somatic cells that lacked AGO2 (34). To investigate whether the delay in CVB3 3A-H57Y replication in the presence of PI4KB inhibitor is due to triggering of antiviral RNAi, we studied its replication kinetics in HeLa and HEK293T cells that lacked AGO2. Similar to our findings in MAVS and PKR knockout cell lines, the delay in replication under PI4KB inhibition was not alleviated in cells lacking AGO2 (Fig. 6D, S5B).

Altogether, these data suggest that the delay in CVB3 3A-H57Y replication under PI4KB inhibition

is not caused by premature triggering of innate antiviral responses as result of impaired RO biogenesis.

AUTHOR CONTRIBUTIONS

Conceptualization: CEM, HMvdS, MB, FJMvK; Investigation: CEM, HMvdS, HRL, RWALL, QF, MW, GJO, MB; Writing: CEM, HMS, MB, FJMvK; Reviewing and editing of the manuscript: CEM, HMS, RPvR, AJK, EJS, MB, FJMvK; Visualization: CEM, HMS; Supervision: HMS, EJS, AJK, RPvR, MB, FJMvK; Funding Acquisition: HMvdS, EJS, RPvR, AJK, MB, FJMvK.

ACKNOWLEDGEMENTS

The authors would like to thank Huib Rabouw for excellent assistance with flow cytometry, and the LUMC light microscopy facility. This work was supported by grants from the Netherlands Organisation for Scientific Research (NWO-VENI-863.12.005 to HMvdS, NWO-VICI-91812628 to FJMvK, ERASysApp project 'SysVirDrug' ALW project 832.14.003 to FJMvK, NWO-MEERVOUD 863.10.003 to MB, NWO-CW TOP 700.57.301 to EJS), and the European Union (7th Framework: EUVIRNA Marie Curie Initial Training Network grant agreement 264286 to FJMvK,; European Research Council Consolidator Grant CoG 615680 to RPvR, Horizon 2020: Marie Skłodowska-Curie ETN 'ANTIVIRALS' grant agreement 642434 to FJMvK). The funders had no role in study design, data collection and interpretation, or the decision to submit the work for publication.

EXPERIMENTAL PROCEDURES

Replication-independent system. HuH-7/T7 cells were seeded in 24-well plates containing glass coverslips. The next day, the cells were lipofectamine transfected with CVB3 cDNA rendered replication-deficient through modifications to the cloverleaf structure in the 5' untranslated region (UTR) of the viral genome (25). One hour later, the medium was replaced with fresh medium. At indicated hours post-transfection, cells were washed and either fixed for immunofluorescence or lysed for Western Blot analysis.

Live cell imaging. BGM(GFPS1-10) cells were grown in glass-bottom 4-chamber 35-mm dishes (CELLviewTM) to ~35% confluency and transduced with MLV mCherry-GM130 particles described before (see (22)). Infection with CVB3 3A-H57Y(S11) was carried out 18-24 hours later. Prior to imaging cells were washed with Fluorobrite medium (Thermo Fisher Scientific) supplemented with 8% fetal calf serum (FCS) and 25 mM HEPES. Cells were maintained in a live-cell imaging chamber at 37°C and 5% CO2. Imaging was carried out from ~2.5 (hpi) using a Leica SP5 confocal microscope. Positions of interest (xyz) were marked and imaged sequentially at 5 minute intervals.

High-pressure freezing and freeze substitution. BGM cells were grown on sapphire discs and infected with CVB3 or CVB3 3A-H57Y and refreshed at 1 hpi with medium supplemented with 25 mM HEPES buffer with or without 1 µm BF738735. Cells were high-pressure frozen using a Leica EM PACT2 at different time points post infection. The instruments and procedures used for freeze-substitution, epoxy resin infiltration and polymerisation were identical to those described in (5). Sections of 70 nm were then prepared for electron microscopy and post-stained with uranyl

acetate and lead citrate.

Correlative light and electron microscopy (CLEM) preparation. BGM (GFPS1-10) cells were cultured in gridded 8-well chamber µ-slides (Ibidi) ahead of infection with CVB3 3A-H57Y(S11). Just prior to imaging cells were treated with 100 nM Mitotracker® Deep Red FM for 30 minutes. Live-cell imaging was carried out to monitor the levels of 3A-H57Y-GFP. High resolution (1024x1024) z-stacks were collected of cells of interest just prior to fixation. To aid in the relocation of these cells for CLEM, tile scan overviews were taken and the positions of cells relative to nearby grid co-ordinates were recorded. Following imaging by live-cell light microscopy (LM), cells were prepared for electron microscopy as described previously (see (22)). EM images were collected of cells previously identified by LM. The EM and LM data for each cell were overlaid using the Mitotracker® Deep Red FM signal (LM images) and corresponding mitochondria (EM images) as a guide for image transformation.

Metabolic labelling and autoradiography. A subconfluent layer of BGM cells was grown in 35 mm dishes (Corning) and infected with CVB3 or CVB3 3A-H57Y at MOI 5. Cells were incubated with dactinomycin for 1 hour prior to a 45-minute labelling with tritiated uridine ([5-3H], 1 mCi/ml) (Perkin Elmer). Cells were processed for EM as described in (22). Sections of 50 nm were collected and post stained with lead citrate and uranyl acetate, then prepared for autoradiography (as described in (51)).

Electron microscopy. Images were collected on an FEI Tecnai12 BioTWIN or TWIN electron microscope at 120 kV using an Eagle 4k slow-scan CCD camera (FEI) or OneView 4k high frame-rate camera (Gatan) respectively. For the collection of larger EM datasets, meshes of overlapping areas across the grid were taken that were later stitched into a single composite image (as described in (52)).

REFERENCES

1. Romero-Brey I, Bartenschlager R. 2014. Membranous Replication Factories Induced by Plus-Strand RNA Viruses. Viruses-Basel 6:2826-2857.
2. Paul D, Bartenschlager R. 2013. Architecture and biogenesis of plus-strand RNA virus replication factories. World J Virol 2:32-48.
3. Schulz KS, Mossman KL. 2016. Viral Evasion Strategies in Type I IFN Signaling - A Summary of Recent Developments. Front Immunol 7:498.
4. White JP, Lloyd RE. 2012. Regulation of stress granules in virus systems. Trends in Microbiology 20:175-183.
5. Limpens RWAL, van der Schaar HM, Kumar D, Koster AJ, Snijder EJ, van Kuppeveld FJM, Barcena M. 2011. The Transformation of Enterovirus Replication Structures: a Three-Dimensional Study of Single- and Double-Membrane Compartments. mBio 2.
6. Belov GA, Nair V, Hansen BT, Hoyt FH, Fischer ER, Ehrenfeld E. 2012. Complex Dynamic Development of Poliovirus Membranous Replication Complexes. Journal of Virology

86:302-312.
7. Suhy DA, Giddings TH, Jr., Kirkegaard K. 2000. Remodeling the endoplasmic reticulum by poliovirus infection and by individual viral proteins: an autophagy-like origin for virus-induced vesicles. J Virol 74:8953-65.
8. Hsu NY, Ilnytska O, Belov G, Santiana M, Chen YH, Takvorian PM, Pau C, van der Schaar H, Kaushik-Basu N, Balla T, Cameron CE, Ehrenfeld E, van Kuppeveld FJM, Altan-Bonnet N. 2010. Viral Reorganization of the Secretory Pathway Generates Distinct Organelles for RNA Replication. Cell 141:799-811.
9. van der Schaar HM, Leyssen P, Thibaut HJ, de Palma A, van der Linden L, Lanke KH, Lacroix C, Verbeken E, Conrath K, Macleod AM, Mitchell DR, Palmer NJ, van de Poel H, Andrews M, Neyts J, van Kuppeveld FJ. 2013. A novel, broad-spectrum inhibitor of enterovirus replication that targets host cell factor phosphatidylinositol 4-kinase IIIbeta. Antimicrob Agents Chemother 57:4971-81.
10. Greninger AL, Knudsen GM, Betegon M, Burlingame AL, Derisi JL. 2012. The 3A protein from multiple picornaviruses utilizes the golgi adaptor protein ACBD3 to recruit PI4KIIIbeta. J Virol 86:3605-16.
11. Altan-Bonnet N, Balla T. 2012. Phosphatidylinositol 4-kinases: hostages harnessed to build panviral replication platforms. Trends Biochem Sci 37:293-302.
12. Dorobantu CM, Albulescu L, Harak C, Feng Q, van Kampen M, Strating JRPM, Gorbalenya AE, Lohmann V, van der Schaar HM, van Kuppeveld FJM. 2015. Modulation of the Host Lipid Landscape to Promote RNA Virus Replication: The Picornavirus Encephalomyocarditis Virus Converges on the Pathway Used by Hepatitis C Virus. Plos Pathogens 11.
13. Clayton EL, Minogue S, Waugh MG. 2013. Mammalian phosphatidylinositol 4-kinases as modulators of membrane trafficking and lipid signaling networks. Progress in Lipid Research 52:294-304.
14. De Matteis MA, Wilson C, D'Angelo G. 2013. Phosphatidylinositol-4-phosphate: the Golgi and beyond. Bioessays 35:612-22.
15. Mesmin B, Bigay J, Moser von Filseck J, Lacas-Gervais S, Drin G, Antonny B. 2013. A four-step cycle driven by PI(4)P hydrolysis directs sterol/PI(4)P exchange by the ER-Golgi tether OSBP. Cell 155:830-43.
16. Arita M. 2014. Phosphatidylinositol-4 kinase III beta and oxysterol-binding protein accumulate unesterified cholesterol on poliovirus-induced membrane structure. Microbiology and Immunology 58:239-256.
17. Strating JRPM, van der Linden L, Albulescu L, Bigay J, Arita M, Delang L, Leyssen P, van der Schaar HM, Lanke KHW, Thibaut HJ, Ulferts R, Drin G, Schlinck N, Wubbolts RW, Sever N, Head SA, Liu JO, Beachy PA, De Matteis MA, Shair MD, Olkkonen VM, Neyts J, van Kuppeveld FJM. 2015. Itraconazole Inhibits Enterovirus Replication by Targeting the Oxysterol-Binding Protein. Cell Reports 10:600-615.
18. Roulin PS, Lotzerich M, Torta F, Tanner LB, van Kuppeveld FJ, Wenk MR, Greber UF. 2014. Rhinovirus uses a phosphatidylinositol 4-phosphate/cholesterol counter-current for the formation of replication compartments at the ER-Golgi interface. Cell Host Microbe 16:677-90.
19. van der Schaar HM, van der Linden L, Lanke KH, Strating JR, Purstinger G, de Vries E, de

Haan CA, Neyts J, van Kuppeveld FJ. 2012. Coxsackievirus mutants that can bypass host factor PI4KIIIbeta and the need for high levels of PI4P lipids for replication. Cell Res 22:1576-92.
20. MacLeod AM, Mitchell DR, Palmer NJ, Van de Poel H, Conrath K, Andrews M, Leyssen P, Neyts J. 2013. Identification of a series of compounds with potent antiviral activity for the treatment of enterovirus infections. ACS Med Chem Lett 4:585-9.
21. Cabantous S, Terwilliger TC, Waldo GS. 2005. Protein tagging and detection with engineered self-assembling fragments of green fluorescent protein. Nature Biotechnology 23:102-107.
22. van der Schaar HM, Melia CE, van Bruggen JA, Strating JR, van Geenen ME, Koster AJ, Barcena M, van Kuppeveld FJ. 2016. Illuminating the Sites of Enterovirus Replication in Living Cells by Using a Split-GFP-Tagged Viral Protein. mSphere 1.
23. Dales S, Eggers HJ, Tamm I, Palade GE. 1965. Electron Microscopic Study of the Formation of Poliovirus. Virology 26:379-89.
24. Belov GA, Feng Q, Nikovics K, Jackson CL, Ehrenfeld E. 2008. A Critical Role of a Cellular Membrane Traffic Protein in Poliovirus RNA Replication. Plos Pathogens 4.
25. Langereis MA, Feng Q, Nelissen FH, Virgen-Slane R, van der Heden van Noort GJ, Maciejewski S, Filippov DV, Semler BL, van Delft FL, van Kuppeveld FJ. 2014. Modification of picornavirus genomic RNA using 'click' chemistry shows that unlinking of the VPg peptide is dispensable for translation and replication of the incoming viral RNA. Nucleic Acids Res 42:2473-82.
26. Molla A, Hellen CU, Wimmer E. 1993. Inhibition of proteolytic activity of poliovirus and rhinovirus 2A proteinases by elastase-specific inhibitors. J Virol 67:4688-95.
27. Ilnytska O, Santiana M, Hsu NY, Du WL, Chen YH, Viktorova EG, Belov G, Brinker A, Storch J, Moore C, Dixon JL, Altan-Bonnet N. 2013. Enteroviruses harness the cellular endocytic machinery to remodel the host cell cholesterol landscape for effective viral replication. Cell Host Microbe 14:281-93.
28. Ford Siltz LA, Viktorova EG, Zhang B, Kouiavskaia D, Dragunsky E, Chumakov K, Isaacs L, Belov GA. 2014. New small-molecule inhibitors effectively blocking picornavirus replication. J Virol 88:11091-107.
29. Arita M. 2016. Mechanism of Poliovirus Resistance to Host Phosphatidylinositol-4 Kinase III beta Inhibitor. Acs Infectious Diseases 2:140-148.
30. Feng Q, Langereis MA, Lork M, Nguyen M, Hato SV, Lanke K, Emdad L, Bhoopathi P, Fisher PB, Lloyd RE, van Kuppeveld FJ. 2014. Enterovirus 2Apro targets MDA5 and MAVS in infected cells. J Virol 88:3369-78.
31. Mukherjee A, Morosky SA, Delorme-Axford E, Dybdahl-Sissoko N, Oberste MS, Wang T, Coyne CB. 2011. The coxsackievirus B 3C protease cleaves MAVS and TRIF to attenuate host type I interferon and apoptotic signaling. PLoS Pathog 7:e1001311.
32. Luna JM, Wu X, Rice CM. 2016. Present and not reporting for duty: dsRNAi in mammalian cells. EMBO J 35:2499-2501.
33. tenOever BR. 2016. The Evolution of Antiviral Defense Systems. Cell Host Microbe 19:142-9.
34. Li Y, Basavappa M, Lu J, Dong S, Cronkite DA, Prior JT, Reinecker HC, Hertzog P, Han Y, Li WX, Cheloufi S, Karginov FV, Ding SW, Jeffrey KL. 2016. Induction and suppression of antiviral RNA interference by influenza A virus in mammalian cells. Nat Microbiol 2:16250.

35. van der Schaar HM, Dorobantu CM, Albulescu L, Strating JR, van Kuppeveld FJ. 2016. Fat(al) attraction: Picornaviruses Usurp Lipid Transfer at Membrane Contact Sites to Create Replication Organelles. Trends Microbiol 24:535-46.
36. Strating JR, van Kuppeveld FJ. 2017. Viral rewiring of cellular lipid metabolism to create membranous replication compartments. Curr Opin Cell Biol 47:24-33.
37. Xu K, Nagy PD. 2014. Expanding use of multi-origin subcellular membranes by positive-strand RNA viruses during replication. Curr Opin Virol 9:119-26.
38. Reghellin V, Donnici L, Fenu S, Berno V, Calabrese V, Pagani M, Abrignani S, Peri F, De Francesco R, Neddermann P. 2014. NS5A Inhibitors Impair NS5A-Phosphatidylinositol 4-Kinase III alpha Complex Formation and Cause a Decrease of Phosphatidylinositol 4-Phosphate and Cholesterol Levels in Hepatitis C Virus-Associated Membranes. Antimicrobial Agents and Chemotherapy 58:7128-7140.
39. Dorobantu CM, Albulescu L, Lyoo H, van Kampen M, De Francesco R, Lohmann V, Harak C, van der Schaar HM, Strating JR, Gorbalenya AE, van Kuppeveld FJ. 2016. Mutations in Encephalomyocarditis Virus 3A Protein Uncouple the Dependency of Genome Replication on Host Factors Phosphatidylinositol 4-Kinase IIIalpha and Oxysterol-Binding Protein. mSphere 1.
40. Reiss S, Rebhan I, Backes P, Romero-Brey I, Erfle H, Matula P, Kaderali L, Poenisch M, Blankenburg H, Hiet MS, Longerich T, Diehl S, Ramirez F, Balla T, Rohr K, Kaul A, Buhler S, Pepperkok R, Lengauer T, Albrecht M, Eils R, Schirmacher P, Lohmann V, Bartenschlager R. 2011. Recruitment and Activation of a Lipid Kinase by Hepatitis C Virus NS5A Is Essential for Integrity of the Membranous Replication Compartment. Cell Host & Microbe 9:32-45.
41. Albulescu L, Wubbolts R, van Kuppeveld FJ, Strating JR. 2015. Cholesterol shuttling is important for RNA replication of coxsackievirus B3 and encephalomyocarditis virus. Cell Microbiol 17:1144-56.
42. Burke JE, Inglis AJ, Perisic O, Masson GR, McLaughlin SH, Rutaganira F, Shokat KM, Williams RL. 2014. Structures of PI4KIIIbeta complexes show simultaneous recruitment of Rab11 and its effectors. Science 344:1035-8.
43. de Graaf P, Zwart WT, van Dijken RA, Deneka M, Schulz TK, Geijsen N, Coffer PJ, Gadella BM, Verkleij AJ, van der Sluijs P, van Bergen en Henegouwen PM. 2004. Phosphatidylinositol 4-kinasebeta is critical for functional association of rab11 with the Golgi complex. Mol Biol Cell 15:2038-47.
44. Dodd DA, Giddings TH, Jr., Kirkegaard K. 2001. Poliovirus 3A protein limits interleukin-6 (IL-6), IL-8, and beta interferon secretion during viral infection. J Virol 75:8158-65.
45. Cornell CT, Kiosses WB, Harkins S, Whitton JL. 2007. Coxsackievirus B3 proteins directionally complement each other to downregulate surface major histocompatibility complex class I. J Virol 81:6785-97.
46. Neufeldt CJ, Joyce MA, Van Buuren N, Levin A, Kirkegaard K, Gale M, Jr., Tyrrell DL, Wozniak RW. 2016. The Hepatitis C Virus-Induced Membranous Web and Associated Nuclear Transport Machinery Limit Access of Pattern Recognition Receptors to Viral Replication Sites. PLoS Pathog 12:e1005428.
47. Welsch S, Miller S, Romero-Brey I, Merz A, Bleck CK, Walther P, Fuller SD, Antony C, Krijnse-Locker J, Bartenschlager R. 2009. Composition and three-dimensional architecture of the

dengue virus replication and assembly sites. Cell Host Microbe 5:365-75.
48. Cortese M, Goellner S, Acosta EG, Neufeldt CJ, Oleksiuk O, Lampe M, Haselmann U, Funaya C, Schieber N, Ronchi P, Schorb M, Pruunsild P, Schwab Y, Chatel-Chaix L, Ruggieri A, Bartenschlager R. 2017. Ultrastructural Characterization of Zika Virus Replication Factories. Cell Rep 18:2113-2123.
49. Bienz K, Egger D, Pfister T, Troxler M. 1992. Structural and functional characterization of the poliovirus replication complex. J Virol 66:2740-7.
50. Lei X, Xiao X, Wang J. 2016. Innate Immunity Evasion by Enteroviruses: Insights into Virus-Host Interaction. Viruses 8.
51. Ginsel LA, Onderwater JJ, Daems WT. 1979. Resolution of a gold latensification-elon ascorbic acid developer for Ilford L4 emulsion. Histochemistry 61:343-6.
52. Faas FG, Avramut MC, van den Berg BM, Mommaas AM, Koster AJ, Ravelli RB. 2012. Virtual nanoscopy: generation of ultra-large high resolution electron microscopy maps. J Cell Biol 198:457-69.

SUPPLEMENTAL EXPERIMENTAL PROCEDURES

Cells. BGM, BGM(GFPS1-10) stably expressing GFP(S1-10) (described in (1)), HeLa R19, HEK293T, U2OS, and HuH-7-Lunet T7-BLR (HuH-7/T7) cells, and a cell pool stably expressing T7 RNA polymerase and blasticidin S-deaminase generously provided by R. Bartenschlager (University of Heidelberg, Heidelberg, Germany) ((2)), were maintained in Dulbecco's modified Eagle's medium (Gibco) supplemented with 10% fetal calf serum, penicillin, and streptomycin, and grown at 37°C in 5% CO2. The culture medium for HuH-77/T7 cells contained 10 µg/ml blasticidine, while that of BGM(GFPS1-10) cells contained 30 µg/ml puromycin.

Knock-out cells. HeLa PKR-/- cells have been described before (see (3)). U2OS PKR-/- were generated using the pCRISPR-hCas9-2xgRNA-Puro plasmid ((4)) with the same gRNAs as used for the HeLa PKR-/- cells, which target the kinase domain of PKR. To target human Ago2, gRNA encoding oligonucleotides cassettes (gRNA1: 5'-ACCGACCGCGTCTGCAATGTGACC-3' and 5'-AACGGTCACATTGCAGACGCGGTC-3', gRNA2: 5'-ACCGCCCATGTTTACAAGTCGGAC-3' and 5'-AACGTCCGACTTGTAAACATGGGC-3') were cloned into the SapI restriction sites of the pCRISPR-hCas9-2xgRNA-Puro plasmid. HEK293T Ago2-/- cells were kindly provided by K.W. Mulder (Radboud University Nijmegen Medical Center, Nijmegen, The Netherlands) and have been described previously (see (5)). To generate HeLa MAVS-/- and U2OS MAVS-/-, cells were co-transfected with two plasmids containing gRNA1 5'- GAATACCCTTCAGCGGCGGCC-3' and gRNA2 5'-GCTGTGAGCTAGTTGATCTCG-3'. Single-cell clones were generated using end-point dilutions. The knock-out was verified by sequence analysis of the genomic DNA and by Western Blot analysis (Fig. S7; HeLa Ago2-/- will be shown elsewhere by RPvR).

Viruses. Coxsackievirus B3 (CVB3) WT was obtained by transfecting in vitro-transcribed RNA derived from the p53CB3/T7 plasmid, which contains the cDNA of CVB3 strain Nancy driven by a T7 RNA polymerase promoter. The 3A-H57Y substitution was introduced in the cDNA clones of CVB3, Rluc-CVB3 and EGFP-CVB3 encoding Renilla luciferase or EGFP upstream of P1 ((6)), or the split-GFP-tagged CVB3 ((1)) using standard DNA cloning techniques. Virus titers were determined by end-

point titration analysis and expressed as 50% cell culture infectious dose (CCID50). A Mengovirus which lost its IFN-suppressing activities due to substitutions in the Zn-finger domain of the leader protein (Mengo Zn) has been described previously (see (7)). Virus titers were determined by end-point titration analysis and expressed as 50% cell culture infectious dose (CCID50).

Reagents. BF738735 (2-fluoro-4-(2-methyl-8-(3-(methylsulfonyl)benzylamino)imidazo[1,2-a] pyrazin-3-yl)phenol) ((8), (9)) was provided by Galapagos NV, used at a working concentration of 1 μM and added in all the experiments 1 hour after infection or mock-infection. Guanidine Hydrochloride (GuHCl) and GW5074 were purchased from Sigma and used at a working concentration of 30 μM and 2 mM respectively. Enviroxime has been previously described ((10)) and used at a concentration of 0.5 μg/ml (1.4 μM). PIK93 was provided by Dr K Shokat (University of California San Francisco, San Francisco, California, USA) and used at a concentration of 1 μM.

Antibodies. The rabbit antiserum and the mouse monoclonal antibody directed against the non-structural protein 3A were described previously (see (11), (12)). Rabbit antiserum against CVB3 3D was generously provided by C.E. Cameron (Pennsylvania State University, USA). Primary mouse monoclonal antibodies included anti-βactin (Sigma Aldrich), anti-GM130 (BD Biosciences), anti-dsRNA J2 (English & Scientific Consulting), and anti-PKR (Santa-Cruz). Primary rabbit polyclonal antibodies included anti-PI4KB (Millipore), anti-TGN46 (Novus Biologicals), anti-phospho-PKR (Abcam), and anti-MAVS (Cardif, Enzo Life Sciences). Alexa Fluor 594-conjugated goat-anti-rabbit IgG and Alexa Fluor 488-conjugated goat-anti-mouse IgG (Molecular Probes) were used as secondary antibodies for immunofluorescence microscopy. For Western Blot analysis, secondary antibody detection included IRDye goat anti-mouse or goat anti-rabbit (LI-COR).

Quantitative PCR. RNA was isolated from infected cells using a Nucleospin RNA kit (Machery-Nagel). cDNA was synthesized using random hexamers as primers with a TaqMan reverse transcription reagents kit (Roche). The cDNA was used for quantitative PCR with the forward primer 5'-CGTGGGGCTACAATCAAGTT-3', the reverse primer 5'-TAACAGGAGCTTTGGGCATC-3', and the LightCycler 480 SYBR Green I master kit (Roche) for 45 cycles (5 s at 95°C, 10 s at 60°C, and 20 s at 72°C) on a LightCycler 480 (Roche). Obtained Ct values were expressed as fold increase with the value at t = 2 h set as 1.

Flow cytometry. BGM cells were seeded in 24-well plates and infected with EGFP-CVB3 3A-H57Y the next day at different MOIs. Cells were released using trypsin, washed once in phosphate buffered saline (PBS), and fixed with 1% paraformaldehyde (PFA) in PBS. Cells were analyzed on FACS Canto (BD) using BD FACS Diva software.

Western Blot analysis. Virus-infected cells were collected in lysis buffer (50 mM TrisHCl pH 7.4, 150 mM NaCl, 1 mM EDTA, 1% Nonidet P-40, 0.05% SDS) and heated for 5 min at 95°C after addition of Laemmli sample buffer. Samples were run on polyacrylamide gels and transferred to a nitrocellulose membrane (Bio-Rad), which following blocking was incubated with primary antibodies overnight at 4˚C and secondary antibodies for 1 h at room temperature. Images of blots were acquired with Odyssey Imaging System (LI-COR).

Immunofluorescence microscopy. BGM cells grown on coverslips were infected with CVB3 WT or CVB3 3A-H57Y for 30-60 minutes, after which the inoculum was removed and fresh medium was added. At indicated time points post-infection, cells were fixed with paraformaldehyde and permeabilized with PBS containing 0.1% Triton X-100. Cells were then stained with primary and secondary antibodies and a nuclear stain (DAPI or Hoechst 33342). Wide-field imaging was

performed using either an Olympus BX60 or Leica DM5500 fluorescent microscope, and confocal imaging was performed with a Leica SpeII confocal microscope.

Replication-independent system. HuH-7/T7 cells were seeded in 24-well plates containing glass coverslips. The next day, the cells were transfected with cDNA of CVB3 rendered replication-deficient through modifications to the cloverleaf structure in the 5' untranslated region (UTR) of the viral genome ((4)) using Lipofectamine 2000 (Thermo Fisher Scientific) according to the manufacturer's protocol. One hour later, the medium was replaced with fresh medium. At indicated hours post-transfection, cells were washed and either fixed for immunofluorescence or lysed for Western Blot analysis.

Live cell imaging. BGM(GFPS1-10) cells were grown in glass-bottom 4-chamber 35-mm dishes (CELLviewTM) to ~35% confluency and transduced with MLV mCherry-GM130 particles described before ((1)). Infection with CVB3 3A-H57Y(S11) was carried out 18-24 hours later. In samples to be studied under PI4KB inhibition, infections were maintained in medium containing 1 µm BF735738 from 1 hpi and for the duration of imaging. Prior to imaging cells were washed with Fluorobrite medium (Thermo Fisher Scientific) supplemented with 8% fetal calf serum (FCS) and 25 mM HEPES. Imaging was carried out from ~2.5 (hpi) using a Leica SP5 confocal microscope equipped with a HyD detector and a 63x (1.4 NA) oil immersion objective, with the confocal pinhole adjusted to 1 airy unit for GFP emission (95.56 µm pinhole). Cells were maintained in a live-cell imaging chamber at 37°C and 5% CO2. Positions of interest (xyz) were marked and imaged sequentially at 5 minute intervals. Live-cell imaging data were processed in ImageJ and aligned using the StackReg plugin.

High-pressure freezing and freeze substitution. BGM cells were grown on sapphire discs and infected with CVB3 or CVB3 3A-H57Y and refreshed at 1 hpi with medium supplemented with 25 mM HEPES buffer. Cells were high-pressure frozen using a Leica EM PACT2 at different time points post infection. The instruments and procedures used for freeze-substitution, epoxy resin infiltration and polymerisation were identical to those described in (13). Briefly, samples were maintained in a Leica AFS2 at -90°C for 44h in a freeze substitution medium containing 10% H20, 2% osmium tetroxide and 1% anhydrous glutaraldehyde. The temperature was then raised to 0°C over a period of 22 hours through a series of controlled warming phases. Samples were washed with acetone, infiltrated with epoxy resin LX-112 (Ladd Research) and polymerised at 60°C. Sections of 70 nm were then prepared for electron microscopy and post-stained with uranyl acetate and lead citrate.

Correlative light and electron microscopy (CLEM). BGM(GFPS1-10) cells were cultured in gridded 8-well chamber µ-slides (Ibidi) ahead of infection with CVB3 3A-H57Y(S11). Cells were maintained in 1 µm BF735738 from 1 hpi in all incubation steps and for the duration of imaging. Just prior to imaging cells were treated with 100 nM Mitotracker® Deep Red FM for 30 minutes, then washed several times in Fluorobrite medium supplemented with 8% FCS and 25 mM HEPES. Images were collected using a Leica SP8 confocal microscope equipped with a HyD detector and using a 63x (1.4 NA) oil immersion objective, while cells were maintained in a live-cell chamber at 37°C and 5% CO2. High resolution (1024x1024) z-stacks were collected of cells of interest. To aid in the relocation of these cells for CLEM, tile scan ((14)) overviews were taken and the positions of cells relative to nearby grid co-ordinates were recorded. Following imaging by live-cell light microscopy (LM), cells were prepared for electron microscopy as described in (1). EM images were collected of cells previously identified by LM. To assess the correlation the EM and LM data for each cell were overlaid (Adobe Photoshop CS6) using the Mitotracker® Deep Red FM signal (LM images) and

corresponding mitochondria (EM images) as a guide for image transformation.

Metabolic labelling and autoradiography. Subconfluent layers of BGM cells were grown in 35 mm dishes (Corning) and infected with CVB3 3A-H57Y at MOI 5 for 1 hour, after which time the incubation medium was replaced with fresh culture medium. Cells were incubated with 10 µg/ml dactinomycin for 1 hour prior to a 45-minute labelling with tritiated uridine ([5-3H], 1 mCi/ml) (Perkin Elmer), after which cells were washed several times to remove unincorporated label and fixed for 1 hour in 1.5% glutaraldehyde in 0.1M cacodylate buffer.. Control samples consisting of uninfected BGM cells pre-treated with dactinomycin and incubated with tritiated uridine were also prepared. Cells were then post-fixed with 1% osmium tetroxide for 1 hour in 0.1M cacodylate buffer followed by a 30 minute incubation with 1% tannic acid in 0.1M cacodylate buffer, after which they were dehydrated in ethanol and infiltrated and embedded in LX 112 resin (Ladd Research Industries) before polymerisation at 60°C. Sections of 50 nm were collected on formvar-coated EM grids and post stained with lead citrate and uranyl acetate, then prepared for autoradiography. For the addition of the layer of photographic emulsion (ILFORD L4), grids were first attached to microscope slides by gently pressing the grid edge against a line of double sided sticky tape applied down the length of the slide, taking care to avoid contact between the tape and the formvar layer. A layer of carbon (~12 nm thick) was then evaporated onto the grids to prevent any direct interaction between the stained epon sections and photographic emulsion, which was subsequently placed on the grids with the help of a wire loop. Samples were developed for autoradiography as described in (15).

SUPPLEMENTAL REFERENCES

1. van der Schaar HM, Melia CE, van Bruggen JA, Strating JR, van Geenen ME, Koster AJ, Barcena M, van Kuppeveld FJ. 2016. Illuminating the Sites of Enterovirus Replication in Living Cells by Using a Split-GFP-Tagged Viral Protein. mSphere 1.
2. Backes P, Quinkert D, Reiss S, Binder M, Zayas M, Rescher U, Gerke V, Bartenschlager R, Lohmann V. 2010. Role of annexin A2 in the production of infectious hepatitis C virus particles. J Virol 84:5775-89.
3. Rabouw HH, Langereis MA, Knaap RC, Dalebout TJ, Canton J, Sola I, Enjuanes L, Bredenbeek PJ, Kikkert M, de Groot RJ, van Kuppeveld FJ. 2016. Middle East Respiratory Coronavirus Accessory Protein 4a Inhibits PKR-Mediated Antiviral Stress Responses. PLoS Pathog 12:e1005982.
4. Langereis MA, Feng Q, Nelissen FH, Virgen-Slane R, van der Heden van Noort GJ, Maciejewski S, Filippov DV, Semler BL, van Delft FL, van Kuppeveld FJ. 2014. Modification of picornavirus genomic RNA using 'click' chemistry shows that unlinking of the VPg peptide is dispensable for translation and replication of the incoming viral RNA. Nucleic Acids Res 42:2473-82.
5. van Eijl R, van den Brand T, Nguyen LN, Mulder KW. 2017. Reactivity of human AGO2 monoclonal antibody 11A9 with the SWI/SNF complex: A case study for rigorously defining

antibody selectivity. Sci Rep 7:7278.
6. Lanke KH, van der Schaar HM, Belov GA, Feng Q, Duijsings D, Jackson CL, Ehrenfeld E, van Kuppeveld FJ. 2009. GBF1, a guanine nucleotide exchange factor for Arf, is crucial for coxsackievirus B3 RNA replication. J Virol 83:11940-9.
7. Hato SV, Ricour C, Schulte BM, Lanke KH, de Bruijni M, Zoll J, Melchers WJ, Michiels T, van Kuppeveld FJ. 2007. The mengovirus leader protein blocks interferon-alpha/beta gene transcription and inhibits activation of interferon regulatory factor 3. Cell Microbiol 9:2921-30.
8. van der Schaar HM, Leyssen P, Thibaut HJ, de Palma A, van der Linden L, Lanke KH, Lacroix C, Verbeken E, Conrath K, Macleod AM, Mitchell DR, Palmer NJ, van de Poel H, Andrews M, Neyts J, van Kuppeveld FJ. 2013. A novel, broad-spectrum inhibitor of enterovirus replication that targets host cell factor phosphatidylinositol 4-kinase IIIbeta. Antimicrob Agents Chemother 57:4971-81.
9. MacLeod AM, Mitchell DR, Palmer NJ, Van de Poel H, Conrath K, Andrews M, Leyssen P, Neyts J. 2013. Identification of a series of compounds with potent antiviral activity for the treatment of enterovirus infections. ACS Med Chem Lett 4:585-9.
10. van der Schaar HM, van der Linden L, Lanke KH, Strating JR, Purstinger G, de Vries E, de Haan CA, Neyts J, van Kuppeveld FJ. 2012. Coxsackievirus mutants that can bypass host factor PI4KIIIbeta and the need for high levels of PI4P lipids for replication. Cell Res 22:1576-92.
11. Wessels E, Duijsings D, Niu TK, Neumann S, Oorschot VM, de Lange F, Lanke KHW, Klumperman J, Henke A, Jackson CL, Melchers WJG, van Kuppeveld FJM. 2006. A viral protein that blocks Arf1-mediated COP-I assembly by inhibiting the guanine nucleotide exchange factor GBF1. Developmental Cell 11:191-201.
12. Dorobantu CM, van der Schaar HM, Ford LA, Strating JRPM, Ulferts R, Fang Y, Belov G, van Kuppeveld FJM. 2014. Recruitment of PI4KIII beta to Coxsackievirus B3 Replication Organelles Is Independent of ACBD3, GBF1, and Arf1. Journal of Virology 88:2725-2736.
13. Limpens RWAL, van der Schaar HM, Kumar D, Koster AJ, Snijder EJ, van Kuppeveld FJM, Barcena M. 2011. The Transformation of Enterovirus Replication Structures: a Three-Dimensional Study of Single- and Double-Membrane Compartments. mBio 2.
14. Faas FG, Avramut MC, van den Berg BM, Mommaas AM, Koster AJ, Ravelli RB. 2012. Virtual nanoscopy: generation of ultra-large high resolution electron microscopy maps. J Cell Biol 198:457-69.
15. Ginsel LA, Onderwater JJ, Daems WT. 1979. Resolution of a gold latensification-elon ascorbic acid developer for Ilford L4 emulsion. Histochemistry 61:343-6.

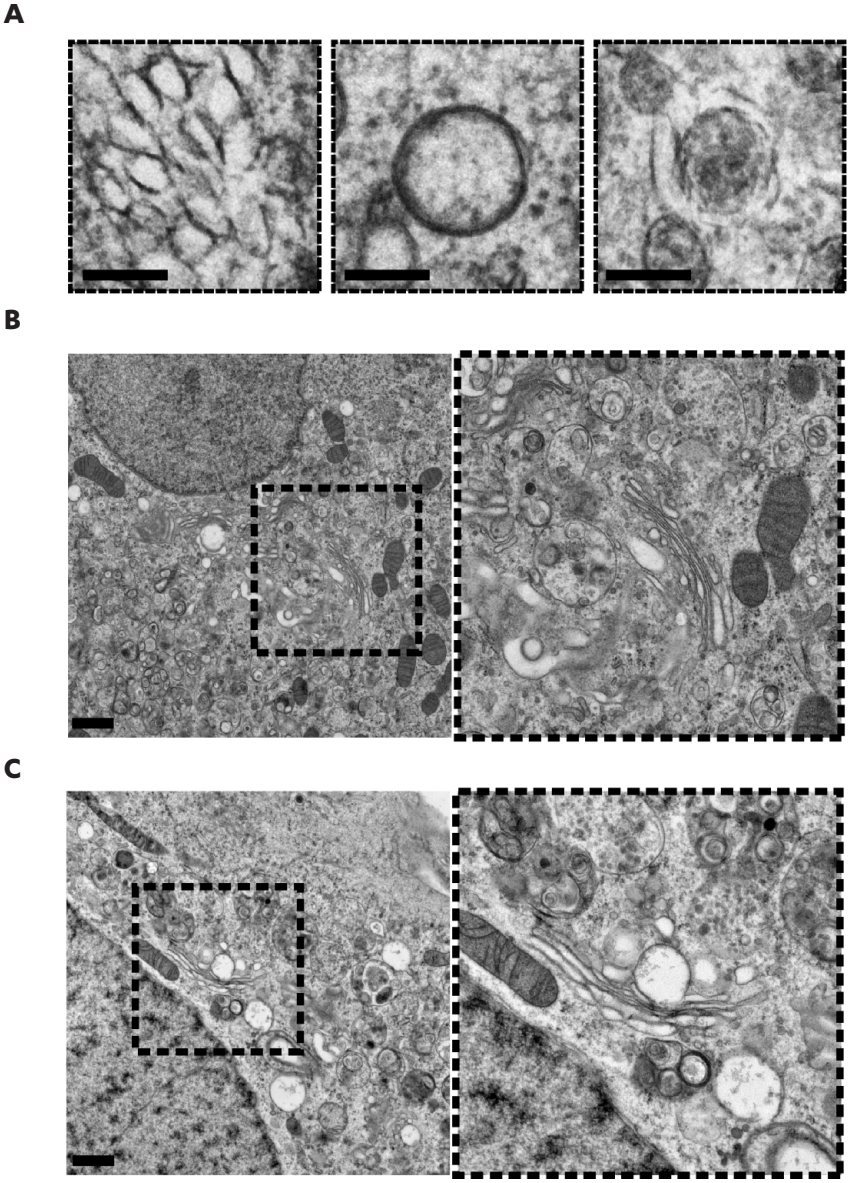

Figure S1. The morphologies of WT CVB3 and CVB3 3A-H57Y ROs in BGM cells are indistinguishable. BF738735 treatment does not affect Golgi apparatus architecture. A) BGM cells infected with WT CVB3 and prepared for EM by HPF-FS reveal typical enterovirus ROs, including single-membrane tubules, DMVs and multilamellar vesicles (left to right). B, C). BGM cells either untreated (B) or treated with BF738735 for 7 hours (C) were fixed for EM analysis. Representative images are shown illustrating that the morphology of the Golgi apparatus was unaffected by treatment. Scale bars, 200 nm (A) or 1 µm (B, C).

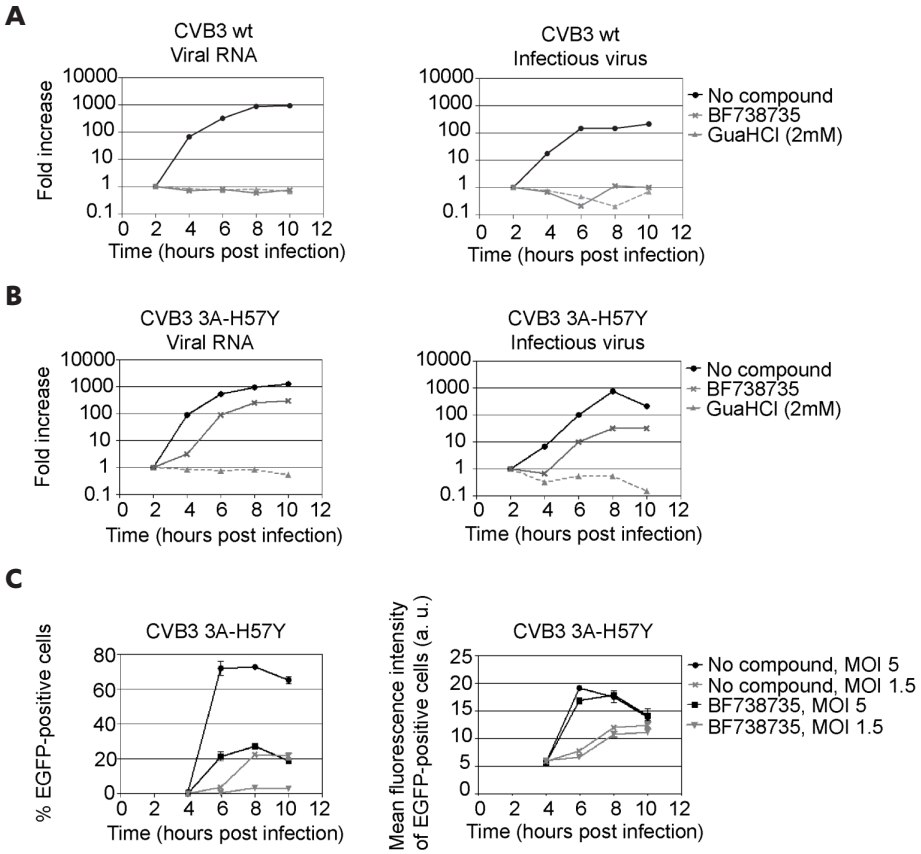

Figure S2. Replication kinetics of CVB3 3A-H57Y differ in the presence or absence of PI4KB inhibitor. A, B) Growth curve analysis. BGM cells were infected with CVB3 WT (A) or CVB3 3A-H57Y (B) and treated with compounds where specified. At the indicated time points, cells were either lysed to determine the intracellular level of viral RNA with quantitative RT-PCR (left graphs), or frozen to titrate the total amount of infectious virus produced (right graphs). Results are expressed as fold increase relative to the quantities at 2 hpi. C) Flow cytometry analysis. BGM cells were infected with EGFP-CVB3 3A-H57Y at different MOIs in the presence or absence of BF738735. At the indicated time points, cells were collected and fixed for flow cytometry analysis to determine the percentage of EGFP-positive cells (left graph) and the mean fluorescence intensity of the EGFP-positive cells (right graph) as an indicator of the level of viral proteins produced. Values represent mean values of triplicates ± standard error of the means.

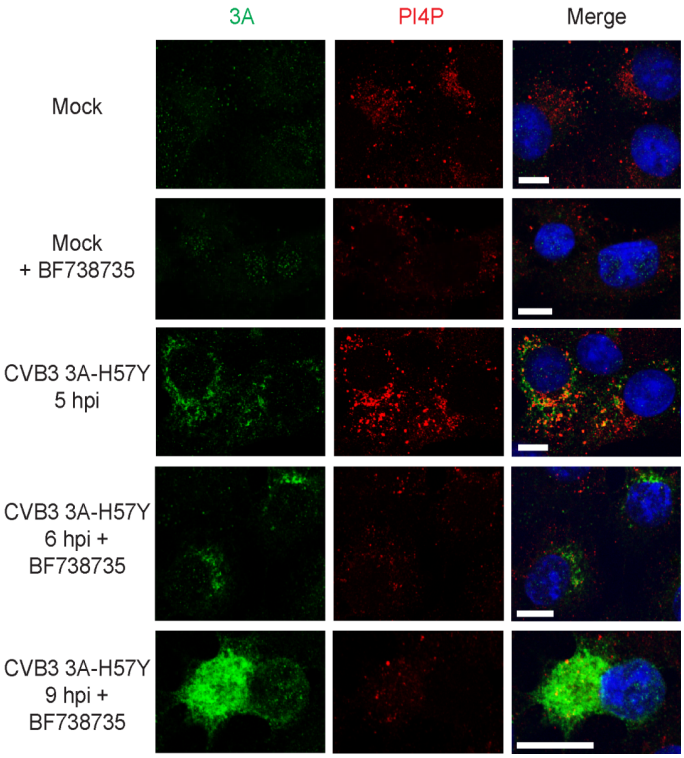

Figure S3. PI4P accumulation is not detected in cells infected with CVB3 3A-H57Y in the presence of PI4KB inhibitor. BGM cells were infected with CVB3 3A-H57Y at MOI 10 and treated with BF738735 where indicated. At the specified time points, cells were fixed and labelled with antibodies against 3A (green) or PI4P (red) alongside a nuclear stain (blue). Confocal images were acquired with a Leica SpeII confocal microscope. Without inhibitor, the level of PI4P signal was considerably elevated (saturated relative to background) in infected cells. In the presence of inhibitor no increase in PI4P was detected in infected cells, even at late time points (9 hpi). Scale bars, 10 µm

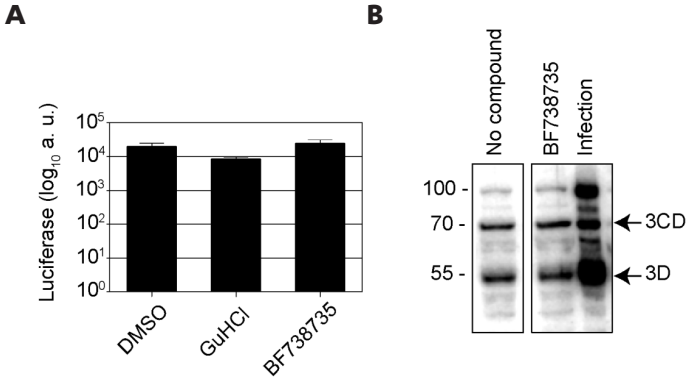

Figure S4. Viral protein production by the replication-independent expression system is not affected by PI4KB inhibition. HuH-7/T7 cells were mock-transfected or transfected with CVB3 3A-H57Y cDNA, which is under the control of a T7 promoter sequence and rendered replication-incompetent by altering the 5'UTR of the genome. cDNA used in (A) additionally encoded Renilla luciferase upstream of the P1 region as a sensitive measure for viral protein production. Cells were treated with BF738735 where indicated. A) At 6 h post transfection, cells were lysed to determine the intracellular luciferase amount. Guanidine Hydrochloride (GuHCl) (2 mM) was used as a positive control for protein production independent of viral RNA synthesis. Values represent mean values of triplicates ± standard error of the means. B) At 7 h post-transfection, cells were lysed and subjected to Western Blot analysis using an antibody against 3D. A lysate of CVB3-infected cells was used as a positive control. Marker bands of the indicated size (in kDa) are indicated.

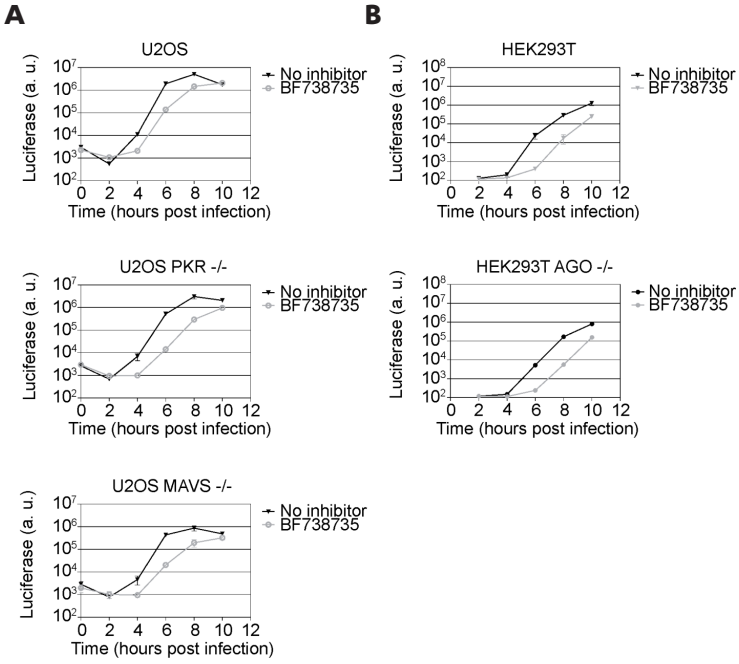

Figure S5. Innate antiviral responses during CVB3 3A-H57Y infection. U2OS or HEK293T cells (KO for PKR, MAVS and AGO where indicated) were infected with CVB3-Rluc 3A-H57Y at MOI 0.01. Following infection, the inoculum was removed and fresh medium with or without BF738735 inhibitor was added to the cells. Cells were lysed to determine the intracellular amounts of luciferase as a measure of genome replication. Values represent mean values of triplicates ± standard error of the means.

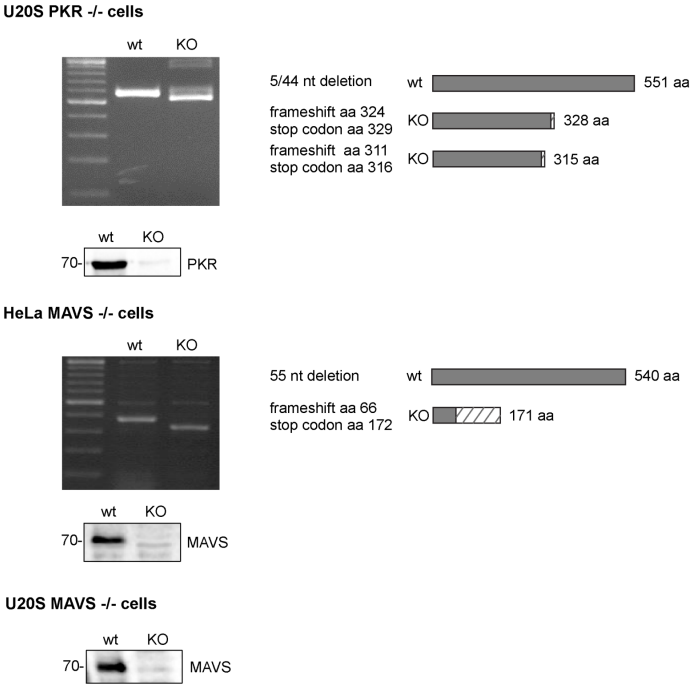

Figure S6. Generation of MAVS-/- and PKR-/- cells using the CRISPR-Cas9 system.
Single-cell clones of HeLa or U2OS cells were characterized by isolation of genomic DNA and PCR with gene-specific primers for PKR or MAVS, followed by sequence analysis (upper panels). All alleles contain a deletion resulting in a frame-shift event and a premature stop codon. The knock-out was confirmed by Western blot analysis of cell lysates (lower panels; marker bands of the indicated size in kDa are indicated on the left). U2OS MAVS-/- cells were only analysed by Western blot.